



CHORUS

This is the accepted manuscript made available via CHORUS. The article has been published as:

Strain-tunable extraordinary magnetocrystalline anisotropy in $\text{Sr}_{\{2\}}\text{CrReO}_{\{6\}}$ epitaxial films

J. M. Lucy, M. R. Ball, O. D. Restrepo, A. J. Hauser, J. R. Soliz, J. W. Freeland, P. M. Woodward, W. Windl, and F. Y. Yang

Phys. Rev. B **90**, 180401 — Published 11 November 2014

DOI: [10.1103/PhysRevB.90.180401](https://doi.org/10.1103/PhysRevB.90.180401)

Strain-tunable, extraordinary magnetocrystalline anisotropy in $\text{Sr}_2\text{CrReO}_6$ epitaxial films

J. M. Lucy¹, M. R. Ball², O. D. Restrepo², A. J. Hauser³, J. R. Soliz⁴,
J. W. Freeland⁵, P. M. Woodward⁴, W. Windl², and F. Y. Yang^{1*}

¹*Department of Physics, The Ohio State University,
191 W. Woodruff Ave., Columbus, Ohio 43210, USA*

²*Department of Materials Science and Engineering,
The Ohio State University, 2041 College Rd., Columbus, Ohio 43210, USA*

³*California Nanosystems Institute, Elings Hall, University of California, Santa Barbara, California 93106, USA*

⁴*Department of Chemistry, The Ohio State University,
100 W. 18th Ave., Columbus, Ohio 43210, USA and*

⁵*Advanced Photon Source, Argonne National Laboratory,
9700 S. Cass Ave., Argonne, Illinois 60439, USA*

(Dated: September 23, 2014)

We report the discovery of extraordinarily large anisotropy fields and strain-tunable magnetocrystalline anisotropy in $\text{Sr}_2\text{CrReO}_6$ epitaxial films. We determine the strain-induced tetragonal distortions and octahedral rotations in $\text{Sr}_2\text{CrReO}_6$ epitaxial films grown on $(\text{LaAlO}_3)_{0.3}(\text{Sr}_2\text{AlTaO}_6)_{0.7}$ (LSAT), SrTiO_3 (STO), and $\text{SrCr}_{0.5}\text{Nb}_{0.5}\text{O}_3$ /LSAT substrates using x-ray diffraction and density functional theory. The structural distortions drive dramatic magnetocrystalline anisotropy. We use magnetometry measurements and first principles calculations to determine the atomic origins of the large anisotropy observed. These techniques elucidate the interplay between structural deformations and magnetic behavior and lay the groundwork for the study of other strongly correlated systems in this class of ferromagnetic oxides.

PACS numbers: 75.30.Gw, 68.55.-a, 71.15.Mb, 78.70.Dm

Magnetocrystalline anisotropy (MCA) has significant implications in a range of applications such as power generation and magnetic data storage. The search for and study of materials for such applications is of both scientific and technological interest. There is much focus on ferromagnets such as SmCo_5 , $\text{Nd}_2\text{Fe}_{14}\text{B}$ and FePt which exhibit high anisotropy due to crystal symmetries and strong spin-orbit coupling [1, 2]. Here we report the discovery of exceptionally large anisotropy fields and strain-tunable MCA in $\text{Sr}_2\text{CrReO}_6$ (SCRO) epitaxial films. We determine the strain-induced tetragonal distortions and octahedral rotations of the SCRO lattice which lead to dramatic changes in MCA and the capability to switch the magnetic easy axis from in-plane to out-of-plane via strain. Furthermore, we perform first principles calculations in order to determine the atomic origins of the large anisotropy observed. This study provides a unique combination of experimental and theoretical work to elucidate atomic magnetic behavior of a complex novel material.

The advances in fabrication techniques of crystalline materials, particularly epitaxial films in recent years, have enabled engineering of materials with desired, and sometimes exotic, electronic and magnetic properties such as new ferroelectric materials [3, 4] and ferromagnets (FMs) with large MCA [1, 2, 5]. Most importantly, epitaxial strain offers the capability to significantly alter the electronic and magnetic properties of the films and even creates new phenomena [3, 4] that do not exist in bulk. Crystal structures that are not isotropic, such as

tetragonal (e.g. CrO_2 and FePt) and hexagonal lattices (e.g. Co and Dy), typically result in large MCA due to magnetization-lattice coupling [5–7]. Since spin-orbit coupling (SOC) generally scales with Z^4 , where Z is the atomic number, high-anisotropy FMs typically contain $4f$ or $5d$ elements. In cubic systems, MCA is usually small due to high crystal symmetry, such as in $3d$ FM metals and Heusler compounds [8, 9].

The ABO_3 perovskites are a large family of complex materials that exhibit many fascinating phenomena. However, magnetic perovskites typically have low T_C and modest MCA. Meanwhile, the $\text{A}_2\text{BB}'\text{O}_6$ ferrimagnetic double perovskites have been shown to possess versatile magnetic properties such as high spin polarization, high T_C (up to 725 K), strong and tunable SOC, and electrical conductivity ranging from insulating to conducting [10–13]. We have demonstrated growth of fully-ordered, high quality SCRO epitaxial films [14–16] using off-axis sputtering, which exhibit SOC-enhanced magnetization. Previous studies of $\text{Sr}_2\text{CrReO}_6$ in bulk and epitaxial film form can be found in Refs. 10, 11, 14–16. It has been recently reported that $\text{Sr}_2\text{CrReO}_6$ films exhibit an abrupt change of magnetic coercivity of 1.2 T when subject to structural transformations of an underlying BaTiO_3 substrate [17]. Theoretical studies also elucidated the contributing factors leading to the large MCA in SCRO [18, 19]. These results point toward the possibility of tuning the large MCA in SCRO films via strain.

We use off-axis sputtering [9, 14–16, 20–23] to deposit 90 nm thick $\text{Sr}_2\text{CrReO}_6$ (001) films on

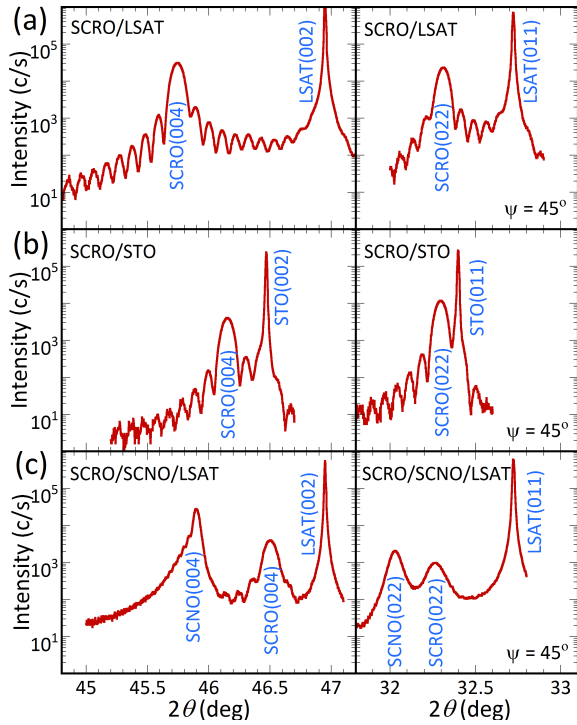


FIG. 1. XRD scans around the $\text{Sr}_2\text{CrReO}_6$ (004) (left panels) and $\text{Sr}_2\text{CrReO}_6$ (022) (right panels) peaks for 90 nm $\text{Sr}_2\text{CrReO}_6$ films grown on (a) LSAT, (b) SrTiO_3 , and (c) a $\text{SrCr}_{0.5}\text{Nb}_{0.5}\text{O}_3$ buffer layer on LSAT. The off-normal $\text{Sr}_2\text{CrReO}_6$ (022) peaks are measured at a tilt angle $\Psi = 45^\circ$ for in-plane characterization.

$(\text{LaAlO}_3)_{0.3}(\text{Sr}_2\text{AlTaO}_6)_{0.7}$ (LSAT), SrTiO_3 (STO), and a relaxed $\text{SrCr}_{0.5}\text{Nb}_{0.5}\text{O}_3$ (SCNO) buffer layer on LSAT with lattice constants $a = 3.868 \text{ \AA}$, 3.905 \AA and 3.946 \AA , respectively (see Supplemental Material for growth parameters). As a comparison, the pseudocubic lattice constants of bulk $\text{Sr}_2\text{CrReO}_6$ are $a_p = 3.907 \text{ \AA}$ and $c_p = 3.905 \text{ \AA}$ [10]. It should be noted that in application it would be favorable to apply continuous strain to the SCRO films through the use of a piezoelectric substrate. However, at this time no piezoelectric substrate is available that can apply epitaxial strain within the approximately $\pm 1\%$ range used here, particularly around the lattice constant of SCRO.

The 90 nm $\text{Sr}_2\text{CrReO}_6$ films are thin enough to be fully strained to the underlying substrates and the similarities in film thicknesses reflect our precise control of deposition rates. The x-ray diffraction (XRD) scans in Fig. 1 show that the films are pure phase with substrate-limited rocking curve full-width-at-half-maximums (FWHMs) as small as 0.0063° . The left panels in Figs. 1(a)-1(c) show the $\theta - 2\theta$ scans near the $\text{Sr}_2\text{CrReO}_6$ (004) peak for films on LSAT, STO and SCNO/LSAT, from which the out-of-plane (perpendicular to the film - substrate interface) lattice constants $c = 7.926 \text{ \AA}$, 7.860 \AA and 7.804 \AA , respectively, are obtained. From the off-axis $\theta - 2\theta$ scans for

the $\text{Sr}_2\text{CrReO}_6$ (022) peak (right panels in Fig. 1), we calculate the in-plane (parallel to the film - substrate interface) lattice constants $a = 7.732 \text{ \AA}$, 7.806 \AA and 7.876 \AA , for films on LSAT, STO and SCNO/LSAT, resulting in tetragonal distortions $c/a = 1.025$, 1.007 and 0.991 , respectively. All three films are fully strained, compressive ($c/a > 1$) or tensile ($c/a < 1$), to the substrates or buffer layer (Table I). Finally, Laue oscillations are observed in all three samples, indicating high uniformity through the films. From the spacing of Laue oscillations, we obtain thicknesses of 91.1, 90.2 and 89.6 nm for the $\text{Sr}_2\text{CrReO}_6$ films grown on LSAT, STO and SCNO/LSAT, respectively.

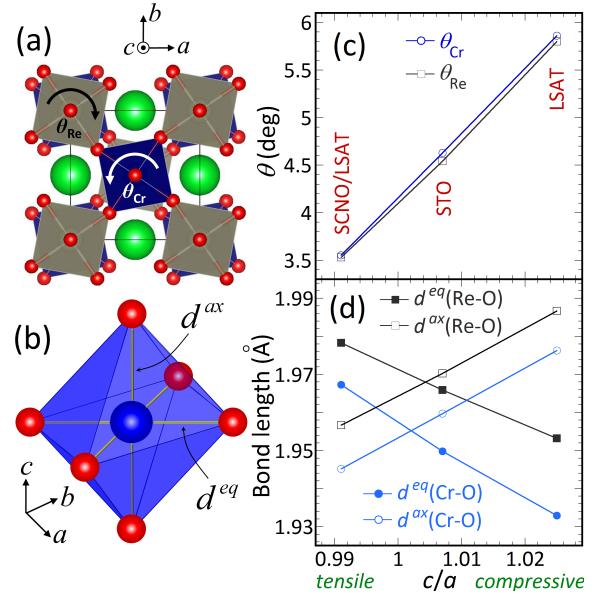


FIG. 2. Schematics of (a) Cr-O (counterclockwise) and Re-O (clockwise) octahedral rotations in the $\text{Sr}_2\text{CrReO}_6$ lattice and (b) an oxygen octahedron surrounding Cr or Re with two different bond lengths, d^{eq} and d^{ax} . (c) Octahedral rotation angle θ and (d) bond lengths of Cr-O and Re-O octahedra as functions of the tetragonal distortion c/a of the $\text{Sr}_2\text{CrReO}_6$ lattice.

In the presence of epitaxial strain, it is energetically favorable for the oxygen octahedra in perovskites to rotate in order to accommodate the tetragonal distortion [24]. Rotation of the octahedra alters both the bond lengths and bond angles between transition metals and oxygen, potentially affecting both their electronic and magnetic properties. We utilize the measured lattice parameters of the SCRO films to determine the rotations of the Cr and Re oxygen octahedra by performing density functional theory (DFT) calculations within the generalized gradient approximation (GGA) [25] using the Vienna *ab initio* simulation package (VASP) [26, 27] with projector augmented wave (PAW) pseudopotentials [28]. Correlation effects were treated within the (GGA+U) approach [29] with a value of $U = 3 \text{ eV}$ and an exchange param-

ter $J = 0.87$ eV for the Cr d -orbitals [30]. The resulting geometries and structural parameters are shown in Fig. 2 and Supplemental Material Table I. As expected, the changes in equatorial (in-plane) and axial (out-of-plane) bond lengths, d^{eq} and d^{ax} , respectively, in the octahedra are considerably smaller than the changes in the lattice constants, accompanied by rotations of the octahedra, as the films undergo progression from compressive to tensile strain. Given the linear relationship in Figs. 2(c) and 2(d), we find that the increase in in-plane bond lengths is 23% (17%) of the changes in the in-plane lattice constant a for Cr (Re) octahedra, while the decrease of the perpendicular bond length is 25% of the change in the value of the c lattice constant for both octahedra. The rotation of the octahedra is similar for both cations and changes by 2.3° across our strain range (Supplemental Material Table I). These structural changes, as shown below, drastically affect the magnetic behaviors of the SCRO films.

To characterize the MCA in our $\text{Sr}_2\text{CrReO}_6$ films, we measure the magnetic hysteresis loops for the three samples in magnetic fields up to 7 T. Fig. 3 shows the in-plane and out-of-plane hysteresis loops at temperatures $T = 20, 100$ and 300 K for the three films after the subtraction of diamagnetic background (see Supplemental Material for diamagnetic background subtraction details). All three substrates (including the buffer layer) exhibit diamagnetic responses at the temperatures discussed in this manuscript.

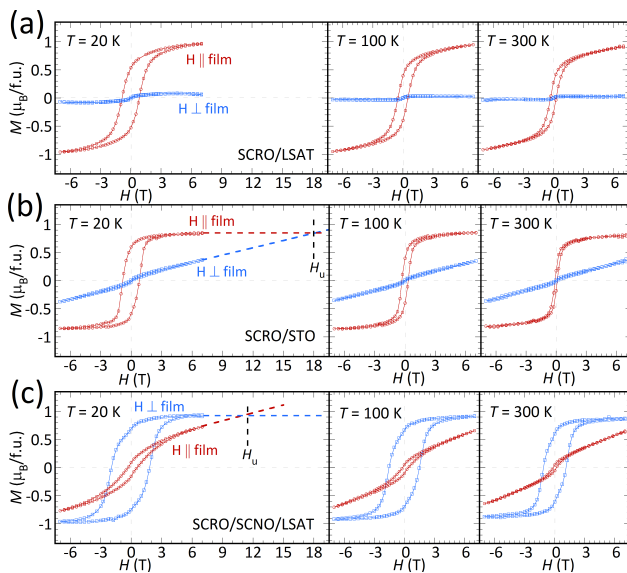


FIG. 3. In-plane and out-of-plane magnetic hysteresis loops for the $\text{Sr}_2\text{CrReO}_6$ films grown on (a) LSAT, (b) SrTiO_3 , and (c) $\text{SrCr}_{0.5}\text{Nb}_{0.5}\text{O}_3/\text{LSAT}$ in magnetic fields up to 7 T at $T = 20, 100$, and 300 K. Magnetic anisotropy fields can be obtained from the intercept of linear extrapolation of the hard-axis hysteresis loops and the saturation magnetization as shown in the left panels.

We note three distinct features from these hysteresis loops. First, the magnetic easy axis changes from in-plane for the films on LSAT and STO with compressive strain ($c/a > 1$) to out-of-plane for the film on SCNO/LSAT with tensile strain ($c/a < 1$). This is similar to the observation in strained $\text{Sr}_2\text{FeMoO}_6$ films [21] since the MCA favors the magnetic easy axis along a shorter axis of the tetragonally distorted crystal lattice. A recent theoretical calculation predicts the change in sign of the MCA energy in $\text{Sr}_2\text{CrReO}_6$ films at a tensile strain of 0.7% using the local-spin-density approximation (LSDA) or 0.3% using the GGA method [18]. For our $\text{Sr}_2\text{CrReO}_6$ film on SCNO/LSAT with a tensile strain of 0.9%, the magnetic easy axis is indeed out-of-plane and complements the theoretical predictions.

Second, the MCA indicated by the hysteresis loops along the hard axis is very large for all three films. In the left panel of Fig. 3(b) for $\text{Sr}_2\text{CrReO}_6/\text{STO}$, we extrapolate the high-field region of the out-of-plane hysteresis loop to find the intercept with the saturation magnetization (M_s) of the in-plane hysteresis loop. This intercept is an approximate representation of the out-of-plane, uniaxial anisotropy field $H_u = 18.1$ T (Table I). Since the magnetization is close to, but not fully saturated at 7 T [14, 31], the obtained H_u from the intercept is an underestimate of the anisotropy field. The demagnetization field $4\pi M_s$ of 1260 Gauss [14] is much smaller than the anisotropy field and can be neglected. We calculate the anisotropy energy by finding the area between the easy and hard axis loops. We find K_u , the uniaxial MCA energy density, to be $K_u = 4.77 \times 10^6$ erg/cm³ (4.77×10^5 J/m³), which is very high for $\text{Sr}_2\text{CrReO}_6$ with a small $M_s = 0.85 \mu_B/\text{f.u.}$ (as a reminder, this is for SCRO/STO). For comparison, SmCo_5 films exhibit one of the highest $K_u = 7.6 \times 10^7$ erg/cm³, while the M_s of SmCo_5 is much higher than that of SCRO [1]. For $\text{Sr}_2\text{CrReO}_6/\text{LSAT}$, the MCA is considerably larger than that in $\text{Sr}_2\text{CrReO}_6/\text{STO}$, as can be seen from the much larger difference between the in-plane and out-of-plane hysteresis loops in Fig. 3(a). The magnetometry data for SCRO/LSAT does not allow reliable determination of H_u from the hysteresis loops since there is very little magnetic signal from the SCRO film for the hard axis loop (see Supplemental Material Figure 1 for the raw magnetic data for SCRO/LSAT). However, we estimate that it should be at least 10's of tesla. For the $\text{Sr}_2\text{CrReO}_6$ film on SCNO/LSAT, the hard axis is in-plane and the anisotropy field $H_u = -11.0$ T is obtained from Fig. 3(c), where the negative sign indicates out-of-plane anisotropy. For this film, we obtain $K_u = -1.46 \times 10^6$ erg/cm³. Clearly, there is a strong dependence of the anisotropy fields on the strain, in particular the c/a ratios of the $\text{Sr}_2\text{CrReO}_6$ films, indicating a strong magnetization-lattice coupling. Using a simple linear extrapolation of the anisotropy fields for the $\text{Sr}_2\text{CrReO}_6$ films on STO ($H_u = 18.1$ T) and SCNO/LSAT ($H_u = -11.0$ T), we

TABLE I. Lattice constants (a, c), tetragonal distortions (c/a), coercivities (H_c), and magnetocrystalline anisotropy fields (H_u) at $T = 20$ K and 300 K of the $\text{Sr}_2\text{CrReO}_6$ films grown on LSAT, SrTiO_3 , and $\text{SrCr}_{0.5}\text{Nb}_{0.5}\text{O}_3/\text{LSAT}$; a_s is the in-plane substrate lattice constant (doubled for LSAT and STO for ease of comparison).

Substrate or Buffer Layer	a_s (Å)	a (Å)	c (Å)	c/a	H_c^{20K} (T)	H_c^{300K} (T)	H_u^{20K} (T)	H_u^{300K} (T)
LSAT	7.736	7.732	7.926	1.025	0.856	0.287	>10's	>10's
SrTiO_3	7.810	7.806	7.860	1.007	0.819	0.113	18.1	16.6
$\text{SrCr}_{0.5}\text{Nb}_{0.5}\text{O}_3/\text{LSAT}$	7.892	7.876	7.804	0.991	1.876	1.128	11.0	11.0

find that the MCA should change sign at 0.30% tensile strain, which agrees with the value predicted by previous GGA calculations [18].

Finally, the anisotropy fields remain essentially unchanged from $T = 20$ to 300 K, which is promising for applications. It should be noted, however, that the coercivity (H_c) decreases with increasing temperature (Table I). This can be understood as follows. The MCA is mainly determined by the magnetic interaction, particularly SOC, and not defects in the films. Since the magnetization of SCRO changes only slightly from 20 to 300 K because of the high T_C [14, 31], the MCA is essentially unchanged below 300 K. Meanwhile, the coercivity is sensitive to defects in the films, thus H_c decreases at higher temperatures due to increasing thermal energy.

To further understand the origin of the change in easy axis under strain seen in experiment, we need to examine the difference in total energies for magnetic orientations along different crystalline axes. This is known as the magnetic anisotropy energy (MAE). The origin of MAE resides in the spin-orbit coupling between the magnetization and the lattice. The crystalline axis associated with the lowest energy determines the most favorable direction of spontaneous magnetization (easy axis). A simple relation between MAE and the moment anisotropy, Δm_L , was proposed by Bruno [32],

$$MAE = -\alpha \frac{\xi}{4\mu_B} \Delta m_L \quad (1)$$

where Δm_L is the difference between hard and easy axis orbital magnetic moments, μ_B is the Bohr magneton, ξ is the spin-orbit coupling constant, and α depends on the electronic structure and is on the order of 0.05-1 [33]. This relation was shown to be valid when the majority spin is fully occupied [32], which is the case for SCRO, and subsequent studies have confirmed it [34–36]. Equation (1) suggests that when the moment anisotropy is calculated for two directions, a sign change in the moment anisotropy indicates a change in easy axis. Performing GGA+U calculations, including spin-orbit coupling, for the different substrate-induced strain states (Supplemental Material Table I), we indeed find that Δm_{tot} (defined as the difference between the magnetic moment in the [001] direction and the average magnetic moment in the [100] and [010] directions) changes sign with increasing

c/a ratio [Fig. 4(a)], in agreement with our experiments (Fig. 3). This agreement confirms the validity of our theory within numerical uncertainties. The calculated Δm_{tot} values are much larger, by 1-2 orders of magnitude, than those found in Ref. 34 for Ni and Fe, demonstrating the robust nature of the magnetic anisotropy in SCRO. However, the Δm_{tot} values are small enough that the precision required to measure them experimentally is not accessible by current magnetometry techniques.

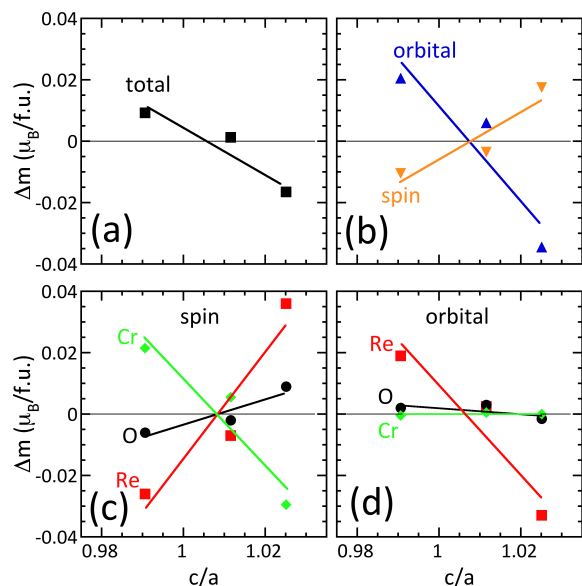


FIG. 4. Differences (Δm) between out-of-plane ([001] direction) and in-plane (average of [100] and [010] directions) (a) total magnetic moments, (b) total orbital and spin magnetic moments, and (c) spin and (d) orbital magnetic moments for Re (squares), Cr (diamonds) and O (circles). The lines are guides for the eye.

Since the easy axis corresponds to the most energetically favorable axis (lowest energy), Eq. (1) tells us that the easy axis aligns with the axis where the orbital magnetic moment is the largest [37]. This overall agreement allows us now to examine the origin of the easy-axis change. For that, we first separate the total moment anisotropy into spin (Δm_S) and orbital (Δm_L) components [Fig. 4(b)] and find that they have approximately linear strain dependence with opposite slopes, with the orbital moment anisotropy dominating. Separating these

contributions further according to their atomic origins, we find that for the spin moment anisotropy [Fig. 4(c)], Cr and Re contribute at approximately the same magnitude, but with opposite sign, thus canceling each other and leaving the small contribution from the hybridizing O atoms as the dominant spin component. We have previously observed experimentally an x-ray magnetic circular dichroism signal at the O K edge (work performed at the Advanced Photon Source, Argonne National Laboratory), complementing our theoretical findings that the O site carries a substantial magnetic moment [38]. The overall dominant orbital moment anisotropy, however, is nearly exclusively imposed by the Re atoms, which contribute 93% to the combined Δm_L [Fig. 4(d)]. The calculated spin and orbital moments for the Cr, Re, and O atoms in SCRO for each strain state (and both in-plane and out-of-plane) can be found in Supplemental Material Table II.

Having identified the Re atoms as the origin of the magnetic anisotropy, we can now look further into the orbital origin of the observed magnetic anisotropy. For that, we examine the changes in calculated Re t_{2g} (xy , yz , and xz) DOS near the Fermi level for tensile ($c/a = 0.99$) and compressive ($c/a = 1.025$) strain (Supplemental Material Figure 3). We observe a downward shift in energy for the xy DOS [Supplemental Material Figure 3(a)] and an upward shift in energy for both yz and xz DOS [Supplemental Material Figure 3(b)] when transitioning from compressive to tensile strain, leading to a change in electron distribution resulting in the observed moment anisotropy.

In conclusion, we reveal large magnetic anisotropy and achieve dramatic changes in the MCA of $\text{Sr}_2\text{CrReO}_6$ films via epitaxial strain. We use DFT calculations to understand the structural distortions and to elucidate the dependence of MCA on the structure of the films. A switching of the magnetic easy axis from in-plane for compressive strain to out-of-plane for tensile strain is observed via SQUID magnetometry and SCRO films exhibit some of the highest anisotropy fields shown to date. Finally, we use first principles calculations to probe the atomic origins of the large and tunable MCA in SCRO, for which the anisotropy is driven primarily by Re orbitals. A thorough understanding of the atomic magnetic behavior of this complex system can guide the design of other versatile and applicable materials. Our results suggest that substitution of other heavy transition metals, such as W or Os, for Re can drastically affect the magnetic properties of FM oxides via tuning of the spin-orbit coupling.

This work is supported by the Center for Emergent Materials at the Ohio State University, a NSF Materials Research Science and Engineering Center (DMR-1420451). Partial support is provided by the NanoSystems Laboratory and the Center for Electron Microscopy and Analysis at The Ohio State University. Work at Argonne National Laboratory, including the Advanced

Photon Source, is supported by the U.S. Department of Energy, Office of Science under Grant No. DEAC02-06CH11357.

* fyyang@physics.osu.edu

- [1] M. Seifert, V. Neu, and L. Schultz, *Appl. Phys. Lett.* **94**, 022501 (2009).
- [2] T. Shima, K. Takanashi, Y. Takahashi, and K. Hono, *Appl. Phys. Lett.* **85**, 2571 (2004).
- [3] J. Haeni, P. Irvin, W. Chang, R. Uecker, P. Reiche, Y. Li, S. Choudhury, W. Tian, M. Hawley, B. Craigo, A. Tagantsev, X. Pan, S. Streiffer, L. Chen, S. Kirchofer, J. Levy, and D. Schlom, *Nature* **430**, 758 (2004).
- [4] J. Wang, J. Neaton, H. Zheng, V. Nagarajan, S. Ogale, B. Liu, D. Viehland, V. Vaithyanathan, D. Schlom, U. Waghmare, N. Spaldin, K. Rabe, M. Wuttig, and R. Ramesh, *Science* **299**, 1719 (2003).
- [5] P. Lukashev, N. Horrell, and R. Sabirianov, *J. Appl. Phys.* **111**, 07A318 (2012).
- [6] D. Behrendt, S. Legvold, and F. Spedding, *Phys. Rev.* **109**, 1544 (1958).
- [7] F. Yang, C. Chien, E. Ferrari, X. Li, G. Xiao, and A. Gupta, *Appl. Phys. Lett.* **77**, 286 (2000).
- [8] G. Daalderop, P. Kelly, and M. Schuurmans, *Phys. Rev. B* **44**, 12054 (1991).
- [9] B. Peters, A. Alfonsov, C. Blum, S. Hageman, P. Woodward, S. Wurmehl, B. Büchner, and F. Yang, *Appl. Phys. Lett.* **103**, 162404 (2013).
- [10] H. Kato, T. Okuda, Y. Okimoto, Y. Tomioka, K. Oikawa, T. Kamiyama, and Y. Tokura, *Phys. Rev. B* **69**, 184412 (2004).
- [11] D. Serrate, J. De Teresa, and M. Ibarra, *J. Phys.: Condens. Matter* **19**, 023201 (2007).
- [12] K.-I. Kobayashi, T. Kimura, H. Sawada, K. Terakura, and Y. Tokura, *Nature* **395**, 677 (1998).
- [13] Y. Krockenberger, K. Mogare, M. Reehuis, M. Tovar, M. Jansen, G. Vaitheeswaran, V. Kanchana, F. Bultmark, A. Delin, F. Wilhelm, A. Rogalev, A. Winkler, and L. Alff, *Phys. Rev. B* **75**, 020404 (2007).
- [14] A. Hauser, J. Soliz, M. Dixit, R. Williams, M. Sumner, B. Peters, L. Mier, T. Gustafson, M. Sumption, H. Fraser, P. Woodward, and F. Yang, *Phys. Rev. B* **85**, 161201 (2012).
- [15] J. Lucy, A. Hauser, H. Wang, J. Soliz, M. Dixit, R. Williams, A. Holcombe, P. Morris, H. Fraser, D. McComb, P. Woodward, and F. Yang, *Appl. Phys. Lett.* **103**, 042414 (2013).
- [16] A. Hauser, J. Lucy, H. Wang, J. Soliz, A. Holcomb, P. Morris, P. Woodward, and F. Yang, *Appl. Phys. Lett.* **102**, 032403 (2013).
- [17] F. Czeschka, S. Gepraegs, M. Opel, S. Goennenwein, and R. Gross, *Appl. Phys. Lett.* **95**, 062508 (2009).
- [18] M. Komelj, *Phys. Rev. B* **82**, 012410 (2010).
- [19] X. Chen, D. Parker, K. Ong, M.-H. Du, and D. Singh, *Appl. Phys. Lett.* **102**, 102403 (2013).
- [20] A. Hauser, R. Williams, R. Ricciardo, A. Genc, M. Dixit, J. Lucy, P. Woodward, H. Fraser, and F. Yang, *Phys. Rev. B* **83**, 014407 (2011).
- [21] C. Du, R. Adur, H. Wang, A. Hauser, F. Yang, and P. Hammel, *Phys. Rev. Lett.* **110**, 147204 (2013).

- [22] H. Wang, C. Du, Y. Pu, R. Adur, P. Hammel, and F. Yang, *Phys. Rev. B* **88**, 100406 (2013).
- [23] C. Du, H. Wang, Y. Pu, T. Meyer, P. Woodward, F. Yang, and P. Hammel, *Phys. Rev. Lett.* **111**, 247202 (2013).
- [24] P. Woodward, *Acta Crystallogr. Sect. B* **53**, 44 (1997).
- [25] J. Perdew, J. Chevary, S. Vosko, K. Jackson, M. Pederson, D. Singh, and C. Fiolhais, *Phys. Rev. B* **46**, 6671 (1992).
- [26] G. Kresse and J. Hafner, *Phys. Rev. B* **49**, 14251 (1994).
- [27] G. Kresse and J. Hafner, *Phys. Rev. B* **47**, 558 (1993).
- [28] P. Blöchl, *Phys. Rev. B* **50**, 17953 (1994).
- [29] V. Anisimov, J. Zaanen, and O. Andersen, *Phys. Rev. B* **44**, 943 (1991).
- [30] H.-T. Jeng and G. Guo, *Phys. Rev. B* **67**, 094438 (2003).
- [31] J. De Teresa, J. Michalik, J. Blasco, P. Algarabel, M. Ibarra, C. Kapusta, and U. Zeitler, *Appl. Phys. Lett.* **90**, 252514 (2007).
- [32] P. Bruno, *Phys. Rev. B* **39**, 865 (1989).
- [33] O. Hjortstam, K. Baberschke, J. M. Wills, B. Johansson, and O. Eriksson, *Phys. Rev. B* **55**, 15026 (1997).
- [34] I. Yang, S. Y. Savrasov, and G. Kotliar, *Phys. Rev. Lett.* **87**, 216405 (2001).
- [35] F. Wilhelm, P. Pouloupoulos, P. Srivastava, H. Wende, M. Farle, K. Baberschke, M. Angelakeris, N. K. Flevaris, W. Grange, J.-P. Kappler, G. Ghiringhelli, and N. B. Brookes, *Phys. Rev. B* **61**, 8647 (2000).
- [36] S. Gold, E. Goering, C. König, U. Rüdiger, G. Güntherodt, and G. Schütz, *Phys. Rev. B* **71**, 220404 (2005).
- [37] H.-T. Jeng and G. Y. Guo, *Phys. Rev. B* **65**, 094429 (2002).
- [38] A. J. Hauser, J. M. Lucy, M. W. Gaultois, M. R. Ball, J. R. Soliz, Y. Choi, O. D. Restrepo, W. Windl, J. W. Freeland, D. Haskel, P. M. Woodward, and F. Yang, *Phys. Rev. B* **89**, 180402 (2014).